The Journal of Pathology: Clinical Research
J Pathol Clin Res March 2025; **11**: e70022
Published online in Wiley Online Library
(wileyonlinelibrary.com). DOI: 10.1002/2056-4538.70022

ORIGINAL ARTICLE

Comprehensive transcriptomic profiling reveals molecular characteristics and biomarkers associated with risk stratification in papillary thyroid carcinoma

Congcong Yan[1†], Chen Zheng[2†], Jiaxing Luo[2], Xue Wu[2], Xinyu Meng[2], Chaoyue Lv[2], Shurong Shen[3], Meng Zhou[1*] and Ouchen Wang[2*]

[1]*School of Biomedical Engineering, Wenzhou Medical University, Wenzhou, PR China*
[2]*Department of Breast Surgery, The First Affiliated Hospital of Wenzhou Medical University, Wenzhou, PR China*
[3]*Department of Surgical Oncology, Wenzhou Central Hospital and Sixth People's Hospital of Wenzhou, Wenzhou, PR China*

**Correspondence to: Meng Zhou, School of Biomedical Engineering, Wenzhou Medical University, Wenzhou 325027, PR China. E-mail: zhoumeng@wmu.edu.cn; Ouchen Wang, Department of Breast Surgery, The First Affiliated Hospital of Wenzhou Medical University, Wenzhou 325027, PR China. E-mail: woc@wmu.edu.cn*

[†]*These authors contributed equally to this work.*

Abstract

Papillary thyroid carcinoma (PTC) is one of the most common endocrine malignancies, with varying levels of risk and clinical behavior. A better understanding of the molecular characteristics could improve molecular diagnosis and risk assessment. In this study, we performed whole transcriptomic sequencing on 113 PTC cases, including 70 high-risk and 43 low-risk Chinese patients. Comparative transcriptional profiling analysis revealed two functionally distinct patterns of gene dysregulation between the risk subtypes. Low-risk PTCs showed significant upregulation of immune-related genes and increased immune cell infiltration, whereas high-risk PTCs presented extensive alterations in gene expression and activation of oncogenic signaling pathways. Additionally, we developed a 31-gene transcriptomic signature (PTCrisk) for differentiating high-risk from low-risk PTCs, which was validated across both in-house and external multicenter cohorts. PTCrisk scores were positively correlated with key clinicopathological features, including tumor size, lymph node metastasis, TNM stage, and *BRAF* mutation status. Overall, our study provides further molecular insights into PTC risk stratification and may contribute to the development of personalized therapeutic strategies for PTC patients.

Keywords: papillary thyroid carcinoma; risk stratification; biomarker; transcriptomics

Received 7 November 2024; Revised 9 January 2025; Accepted 7 February 2025

No conflicts of interest were declared.

Introduction

Thyroid cancer is one of the most prevalent endocrine malignancies, with an increasing incidence worldwide over the past few decades [1]. According to the International Agency for Research on Cancer, thyroid cancer accounted for 3–4% of all cancer cases, making it the ninth most common cancer globally in 2020 [2]. The World Health Organization (WHO) classifies thyroid cancer into four main histological subtypes: papillary (PTC), follicular, poorly differentiated, and anaplastic thyroid cancers, with PTC accounting for approximately 85% of cases [3]. PTC is generally characterized as an indolent tumor with slow progression [4]. Postoperative interventions, such as surgery or radioactive iodine treatment, can yield a 5-year survival rate exceeding 90% for most PTC patients [5]. However, a subset of patients remains at high risk for metastasis and recurrence, with cervical lymph node metastasis rates ranging from 60% to 70% [6]. High-grade differentiated thyroid carcinoma (DTC) is a distinct subset of differentiated thyroid cancers with more aggressive clinical behavior. Despite retaining some differentiation features, high-grade DTC is marked by increased mitotic activity, necrosis, and vascular invasion, contributing to higher rates of

recurrence and metastasis and poorer outcomes [7,8]. Therefore, it is of utmost importance to further investigate the molecular characteristics of PTC with different risk behaviors and to tailor individualized treatment strategies.

Over the last decade, a thyroid classification system has been progressively established to estimate the likelihood of ongoing thyroid cancer after initial treatment, focusing on the risk of recurrence [9]. Clinically, the initial diagnosis of thyroid lesions is achieved through a comprehensive clinical evaluation and various imaging techniques [10]. The preliminary assessment should be the basis for the decision on the appropriate first-line treatment, such as lobectomy, total thyroidectomy, or active surveillance [11]. In 2015, the American Thyroid Association introduced a three-level clinicopathological risk stratification system for customized thyroid care, categorizing PTC patients into low-, intermediate-, and high-risk groups for recurrence [12]. Despite these stratifications, distinguishing high-risk from low-risk PTC patients based solely on postoperative pathological reports remains challenging.

In this study, we aimed to comprehensively explore the molecular and immunological features of PTC by analyzing the transcriptomic profiles of high- and low-risk patients. We identified potential diagnostic and prognostic biomarkers for PTC risk stratification and validated them in independent cohorts to confirm the robustness of our findings.

Materials and methods

Patients and samples

A total of 113 PTC patients who underwent radical thyroidectomy were retrospectively collected in the First Affiliated Hospital of Wenzhou Medical University (WMU) from 2019 to 2020. The 113 PTC patients were allocated to two cohorts according to a 7:3 ratio: the WMU-1 cohort ($n = 80$) for discovery and the WMU-2 cohort ($n = 33$) for validation. The pathological results of all tissues were confirmed by two expert pathologists. Surgically removed thyroid tissue was immediately and rapidly frozen in liquid nitrogen and then stored at −80°C for subsequent RNA extraction. In addition, none of the enrolled patients received preoperative treatment such as preoperative chemotherapy or radiation therapy. The detailed clinical information for the patients is shown in Table 1. This study was approved by the Ethics Committee of the First Affiliated Hospital of Wenzhou Medical University (YS2022-472). Written informed consent was obtained from all the patients before enrollment.

Assessment of PTC risk

The criteria for categorizing patients into the high-risk group for thyroid cancer were as follows: (1) the presence of tumor metastases in both central and lateral

Table 1. Clinical characteristics of PTC patients enrolled in this study

Characteristics	WMU-1 cohort			WMU-2 cohort		
	High risk ($N = 49$)	Low risk ($N = 31$)	p	High risk ($N = 21$)	Low risk ($N = 12$)	p
Age, median (range)	45.00 (33.00–54.00)	44.00 (36.00–52.00)	0.969*	46.00 (32.00–54.00)	48.00 (34.00–58.50)	0.631*
Gender			0.008†			<0.001†
Male	20	4		17	0	
Female	29	27		4	12	
Tumor size (mm)			0.006†			0.042†
≥20	16	2		8	0	
<20	33	29		13	12	
Multi-nodularity			0.073†			0.866†
Yes	26	22		12	8	
No	23	9		9	4	
Lymph-node metastasis			<0.001†			<0.001†
CLNM	48	0		21	0	
LLNM	0	0		0	0	
No	1	31		0	12	
BRAF status			0.055†			0.851†
Positive	32	20		15	7	
Negative	4	3		2	1	
NA	13	8		4	4	

CLNM, central lymph node metastasis; LLNM, lateral lymph node metastasis.
*Mann–Whitney *U* test.
†χ^2 test.

cervical lymph nodes, with a metastatic rate exceeding 50%; (2) the presence of five or more metastatic lymph nodes in the central compartment; (3) tumor size of 4 cm or larger, accompanied by a lymph node metastatic rate exceeding 50%; (4) extrathyroidal glandular invasion by the tumor; (5) patients with aggressive histological tumor subtypes; (6) patients with distant metastases; and (7) patients undergoing postoperative I^{131} therapy. Conversely, the definition criteria for the low-risk group in thyroid cancer were delineated as follows: (1) at least seven central lymph nodes removed, with none showing metastatic involvement; (2) the total number of lymph nodes excised from both central and lateral neck compartments was at least 10, with at least two nodes from each compartment, and no metastasis detected in any node; (3) tumor diameters were equal to or smaller than 2 cm; (4) there was no evidence of capsular or extrathyroidal glandular invasion; (5) absence of distant metastases or lymph node recurrence; and (6) post-total thyroidectomy, patients should not exhibit sustained elevations in thyroglobulin levels.

Library construction and whole transcriptome sequencing

The RNA libraries were prepared using the NEB Next® Ultra™ II DNA Library Prep Kit (Illumina, Inc., San Diego, CA, USA) in conjunction with the high-throughput MGI SP-960 sample prep system according to the manufacturer's protocols. Ribosomal RNA (rRNA) was effectively removed from the samples using the Epicentre® Ribo-zero rRNA Removal Kit (Epicentre, Illumina) following the manufacturer's recommendations. The RNA samples were then prepared for downstream processing by ligating 3′- and 5′-adapters, followed by reverse transcription utilizing an RT primer, which introduced sample-specific barcodes for identification purposes.

The resultant cDNA fragments, targeted to span 370–420 bp, were size-selected and purified using AMPure Beads XP (Beckman Coulter, Indianapolis, IN, USA). The purified PCR products, diluted to 1.5 ng/μL, were then assessed for size using the Agilent 2100 Bioanalyzer (Agilent Technologies, Santa Clara, CA, USA), and their concentrations were determined with the Qubit 2.0 Fluorometer (Thermo Fisher Scientific, Waltham, MA, USA). Only RNA samples fulfilling the stringent criteria (RNA ≥ 1.0 μg, concentration ≥ 50 ng/μL, and OD260/280 ≥ 1.8) proceeded to data analysis.

After the library was confirmed, sequencing was conducted on the Illumina NovaSeq 6000 platform, generating paired-end reads of 150 bp. Data quality control involved converting high-throughput sequencer image data into sequence data (Reads) through CASAVA base calling. Initial processing of the raw fastq format data utilized in-house Perl scripts to remove adapter sequences, N bases, and low-quality reads, producing clean data (clean reads). Q20, Q30, and GC content were also computed. The sequencing data for each sample was expected to comprise at least 50 million reads with a raw data size of ≥15G, with quality thresholds of Q20 ≥90% and Q30 ≥85%. Additionally, the sequencing output for each sample should not deviate by more than 2% from the average data yield across all samples.

Gene and transcript annotations

All whole transcriptome analyses conducted in this study utilized the human genome hg38 reference assembly. The results were extensively annotated to include known gene and transcript identifiers and their genomic locations wherever possible. Upon completion of transcript assembly, gene symbols were systematically assigned Ensembl IDs, predicated on their locational concordance with established transcripts, with a required minimum overlap threshold of 90%. In cases where overlapping failed, custom and unique IDs were employed to assign gene symbols during the transcript assembly process. The gene and transcript assignments were based on the Ensembl GRCh38 annotations available in both core and funcgene databases, version 104.

Public patient and transcriptome data

An additional 611 PTC samples and the corresponding clinical and transcriptomic data were retrieved from The Cancer Genome Atlas (TCGA; https://xenabrowser.net/) and the Gene Expression Omnibus (GEO; https://www.ncbi.nlm.nih.gov/geo), including 495 samples from TCGA, 65 samples from GSE35570, and 51 samples from GSE27155 [13,14]. Raw microarray data were normalized using the robust multiarray average method with R package 'affy' [15].

Biomarker identification and model development for risk stratification

To remove uninformative variables, variables with a coefficient of variation lower than 0.2 and constant or almost constant value were removed using the function nearZeroVar in the R package 'caret' [16]. To identify risk-associated biomarkers, differential expression analysis was performed between low- and high-risk samples using R package 'DESeq2' and p values were

adjusted using the false discovery rate (FDR) method [17]. Those mRNAs with FDR below 0.05 were designated as differentially expressed genes (DEGs). From the DEG pool, least absolute shrinkage and selection operator (LASSO) regression was performed to refine the set of predictive features.

A risk predictive model was constructed utilizing the random forest algorithm with a 10-fold cross-validation procedure to accurately differentiate between low- and high-risk patients with PTC. The model assigns risk scores between 0 and 1, representing the estimated risk probability for each patient. A threshold of 0.5 was established, with scores above this threshold indicating a high risk of PTC and scores below it indicating a low risk.

Functional analysis

Gene ontology (GO) enrichment analysis was conducted to elucidate the biological processes of interested gene sets, using the Cytoscape software integrated with the ClueGO plugin for visualization [18,19]. The semantic similarity of GO terms between GO terms was quantified and represented graphically through the R package 'simplifyEnrichment' [20]. Kyoto Encyclopedia of Genes and Genomes (KEGG) enrichment analysis was performed to identify significantly enriched pathways using the R package 'clusterProfiler' [21].

The 29 functional gene expression signatures (Fges) and hallmark gene sets were obtained from the study by Newell *et al* and the Molecular Signatures Database, respectively [22,23]. The enrichment scores of hallmark gene sets and Fges were calculated for each sample via single-sample Gene Set Enrichment Analysis (ssGSEA) using the 'GSVA' R package [24–26]. The state of anti-cancer immunity across the seven-step cancer-immunity cycle was analyzed via Tracking Tumor Immunophenotype (http://biocc.hrbmu.edu.cn/TIP/).

Statistical analysis

Statistical differences between the two groups of continuous variables or categorical variables were determined using the Mann–Whitney *U* test or Fisher's exact test, respectively. Diagnostic performance was assessed using the receiver operating characteristic (ROC) curves and area under the curve (AUC) with R package 'pROC'. Survival differences between groups were evaluated using the Kaplan–Meier method complemented by the log-rank test. The effects of candidate genes on patient survival were examined by the univariate Cox proportional hazards regression model. The performance of prognostic biomarkers is evaluated using the time-dependent ROC curves and AUCs with the 'timeROC' R package. All statistical analyses were conducted in R version 4.0.

Results

Study populations and patient characteristics

All 113 PTC patients were divided into two distinct cohorts: the first, referred to as the WMU-1 cohort, consisted of 31 low-risk and 49 high-risk patients, and the second, named the WMU-2 cohort, comprised 12 low-risk and 21 high-risk individuals (Figure 1A). The clinical characteristics of the participants are summarized in Table 1. In the WMU-1 cohort, the median ages for the high-risk and low-risk groups were 45 years (range: 33–54 years) and 44 years (range: 36–52 years), respectively, indicating no statistically significant difference ($p = 0.969$). The WMU-2 cohort exhibited a similar age distribution, with median ages of 46 years (range: 32–54 years) for the high-risk group and 48 years (range: 34–58.5 years) for the low-risk group, again showing no significant age disparity ($p = 0.631$). Despite comparable age distributions, there were significant disparities in sex distribution and tumor size within both cohorts ($p < 0.05$). Notably, the high-risk groups in both cohorts demonstrated a significantly higher prevalence of central lymph node metastases (CLNM) compared to the low-risk groups ($p < 0.001$). However, factors such as multinodularity and *BRAF* mutation status did not exhibit significant differences between the groups in either cohort ($p > 0.05$).

Distinct transcriptomic profiles of low-risk and high-risk PTC

To investigate transcriptomic alteration associated with risk stratification in PTC, we performed next-generation sequencing to profile mRNA expression in 31 low-risk and 49 high-risk PTC specimens (Figure 1A). To identify specific genes implicated in the heterogeneous pathologies characteristic of different risk subtypes, we performed differential expression analysis of transcriptomic profiles between low-risk and high-risk PTC groups using DESeq2. We identified a total of 583 DEGs with the selection criterion of an FDR-adjusted p value less than 0.05, distinguishing between high-risk and low-risk PTCs (Figure 1B and supplementary material, Table S1). Among these DEGs, 210 genes were identified as significantly upregulated,

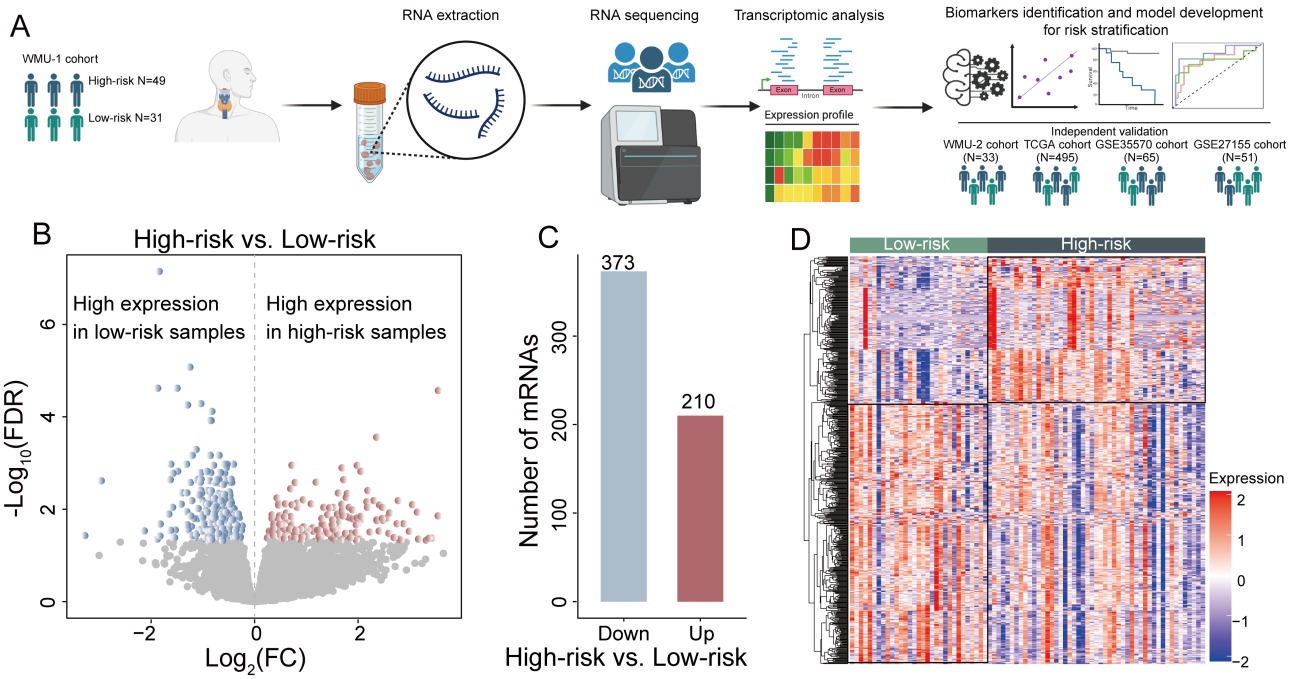

Figure 1. Transcriptional landscape of high-risk and low-risk papillary thyroid cancer. (A) Overview of the study design and workflow. Our study aimed to characterize low-risk and high-risk PTC and identify diagnostic and prognostic biomarkers. Created with BioRender (https://www.biorender.com/). (B) Volcano plot showing $\log_2$ fold change and FDR-adjusted p values between high- and low-risk patients. Differentially expressed genes in high-risk (red) and low-risk (blue) groups are shown. (C) Comparing high-risk samples to low-risk samples, the numbers of significantly downregulated and upregulated mRNAs are shown in the blue and red bars respectively. (D) Unsupervised clustering using the expression pattern of differentially expressed genes.

whereas 373 were found to be downregulated in the high-risk PTC compared to low-risk PTC (Figure 1C). Hierarchical clustering further delineated that these DEGs distinctly segregated high-risk from low-risk PTCs, demonstrating the potential of transcriptomic profiling for risk stratification in PTCs (Figure 1D).

Characterization of perturbed biological and immunological features in low-risk and high-risk PTC

We next explored the perturbed biological processes and signaling pathways distinguishing low-risk from high-risk PTC. We first performed GO functional enrichment analysis for DEGs and observed a prevalence of immune-related biological processes (Figure 2A). Pathway enrichment analysis further supported these findings, showing consistent results with the GO analysis (Figure 2B). Additionally, we conducted gene set enrichment analysis for the 50 cancer hallmark gene sets. By comparing the enrichment scores of high-risk and low-risk patients, we observed that high-risk PTC samples exhibited significant enrichment of cancer hallmark pathways compared to the low-risk group (Figure 2C). Furthermore, we found strong positive correlations between hallmark gene modules, indicating coordinated alterations in these pathways in the high-risk group (Figure 2D). These results collectively suggest the presence of distinct underlying molecular mechanisms between low-risk and high-risk PTC subtypes, particularly with regard to immune-related processes and cancer hallmark pathways.

Given the identified immune process enrichment among DEGs, we further explored the immune characteristics between low-risk and high-risk PTC. We conducted a comprehensive comparison of 29 Fges, infiltrating immune cell populations, and the cancer-immunity cycle using the ssGSEA analysis. As shown in Figure 2E, the low-risk PTCs were found to exhibit significantly higher pro-tumor immune and anti-tumor immune scores compared with the high-risk group, as determined by the Mann–Whitney U test ($p < 0.05$). Pearson correlation analysis indicated a significant positive relationship between pro-tumor immune and anti-tumor immune scores (supplementary material, Figure S1A). Further detailed analysis of the

abundance of 28 immune cell subpopulations using ssGSEA demonstrated that the low-risk group was characterized by significantly higher levels of adaptive and activated immune cell infiltration, particularly T-cell infiltration (supplementary material, Figure S1B). Moreover, the infiltration of various

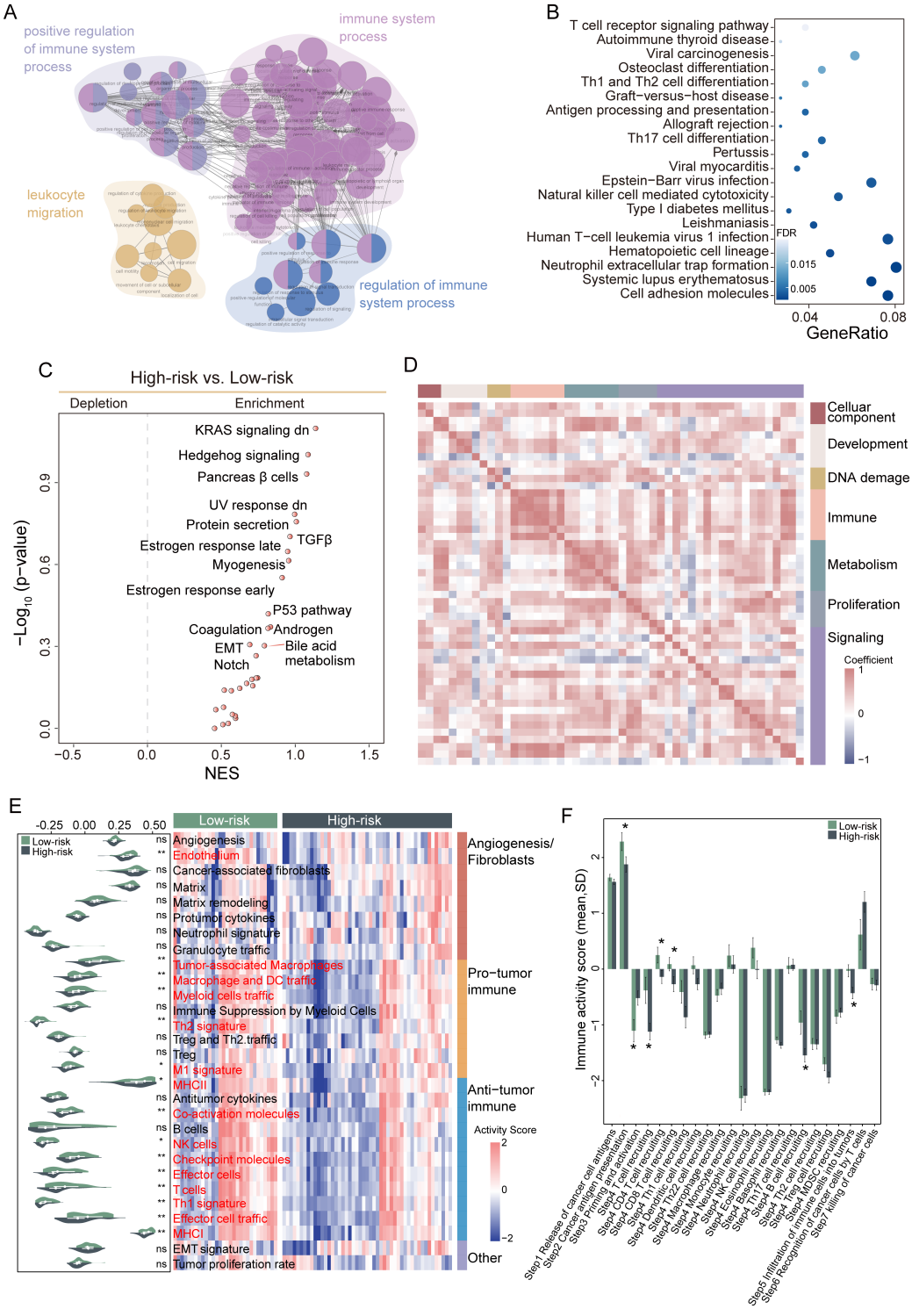

Figure 2. Legend on next page.

T-cell subtypes showed positive correlations with each other (supplementary material, Figure S1C). An examination of the cancer-immunity cycle stages revealed significant differences between the low-risk and high-risk groups, with the low-risk group displaying pronounced anti-cancer immune activities including cancer antigen presentation (Step 2), the trafficking of immune cells to tumors (Step 4) (such as CD8/CD4 T-cell recruiting and B-cell recruiting), and enhanced infiltration of immune cells into tumors (Step 5) (Figure 2F). These findings collectively suggest that the low-risk group promotes an immune-inflamed phenotype and stimulates the infiltration of diverse T-cell subsets, indicating a more robust anti-cancer immune response compared to the high-risk group.

Identification of potential biomarkers for differentiating high-risk and low-risk PTCs

To identify critical genes serving as diagnostic biomarkers for categorizing PTC into high-risk or low-risk groups, we conducted machine learning-based feature selection with LASSO regression analysis and identified 31 key genes with non-zero coefficients (Figure 3A,B). KEGG enrichment analysis revealed that these genes were enriched in cell growth, taurine and hypotaurine metabolism (Figure 3C). Similarly, GO enrichment analysis highlighted their association with biological processes involved in biosynthesis and development (Figure 3D).

Then we developed a machine learning classification model, termed 'PTCrisk', using the random forest technique based on the expression pattern of these 31 key genes. PTCrisk is designed to allocate a risk probability ranging from 0 to 1 for each PTC case. In the WMU-1 cohort, patients were stratified into high-PTCrisk or low-PTCrisk groups based on a cutoff value of 0.5. Remarkably, PTCrisk precisely classified 31 PTC samples as low-risk and 49 as high-risk, achieving an AUC of 1.0 (Figure 3E). High-risk PTC samples exhibited significantly higher risk scores compared to low-risk samples (Mann–Whitney U test, $p < 0.001$) (Figure 3F,G). We further examine the association of PTCrisk with clinicopathological parameters of PTC aggressiveness using the Pearson correlation coefficients. The analysis revealed significant correlations of PTCrisk with larger tumor diameter ($R = 0.38$, $p < 0.001$), higher lymph node metastasis rates ($R = 0.88$, $p < 0.001$), CLNM rates ($R = 0.91$, $p < 0.001$), and lateral lymph node metastasis rates ($R = 0.74$, $p < 0.001$), respectively (Figure 3H–K). Comparative analyses also demonstrated that the high-PTCrisk group presented significantly higher tumor diameters and metastasis rates compared to the low-PTCrisk group (Figure 3H–K).

Independent internal validation of PTCrisk in the in-house cohort

To evaluate the reliability and robustness of PTCrisk, we applied it to an independent internal validation cohort (WMU-2 cohort) from our institution, consisting of 21 high-risk PTC and 12 low-risk PTC cases. Consistent with the results from the discovery cohort, PTCrisk effectively distinguished high-risk from low-risk PTC, achieving an AUC of 0.84 (95% CI: 0.68–0.99; Figure 4A). The risk scores were significantly higher in the high-risk group compared to the low-risk group. As shown in Figure 4B,C, the high-risk group exhibited significantly higher PTCrisk scores than the low-risk group. Given that previous studies have identified age >55 years as an indication of a higher risk of thyroid cancer recurrence [27,28], we further divided the samples into two age groups: <55 and ≥55 years. Once again, PTCrisk effectively distinguished high-risk patients from low-risk patients, yielding an AUC of 0.90 (95% CI: 0.78–1) for patients aged <55 and an AUC of 0.67 (95% CI: 0.01–1) for those aged ≥55 (Figure 4D). Correlation analyses between PTCrisk scores and clinicopathological features in the WMU-2

Figure 2. Comparison of immunological features between the high-risk and low-risk groups. (A) Visualization of functionally grouped networks with significantly enriched GO functional terms as nodes, where larger node size indicates more significant enrichment. (B) The top enriched pathways of dysregulated genes. The point size and color represent the number of DEGs in the pathway and the significance level. (C) Volcano plots showing the enrichment of hallmark gene sets for high-risk and low-risk groups calculated based on the normalized enrichment score from GSEA. (D) Pearson correlations among hallmark gene set enrichment scores are shown, with correlations shown in blue and red depending on whether they are negative or positive. (E) Heatmap and violin plots of ssGSEA enrichment scores of functional gene expression signatures for each sample in two groups. (F) Immune activity scores of cancer-immunity cycle steps in high-risk and low-risk samples, respectively. Data are presented as the mean and SD. The data are analyzed using the Mann–Whitney U test. SD, standard deviation. FC, fold change; FDR, false discovery rate; NES, normalized enrichment score.

cohort revealed correlations with tumor diameter ($R = 0.35$), lymph node metastasis rates ($R = 0.49$), CLNM rates ($R = 0.54$), and lateral lymph node metastasis rates ($R = 0.23$), with significantly higher clinical parameters observed in the high-PTCrisk group (Figure 4E–H).

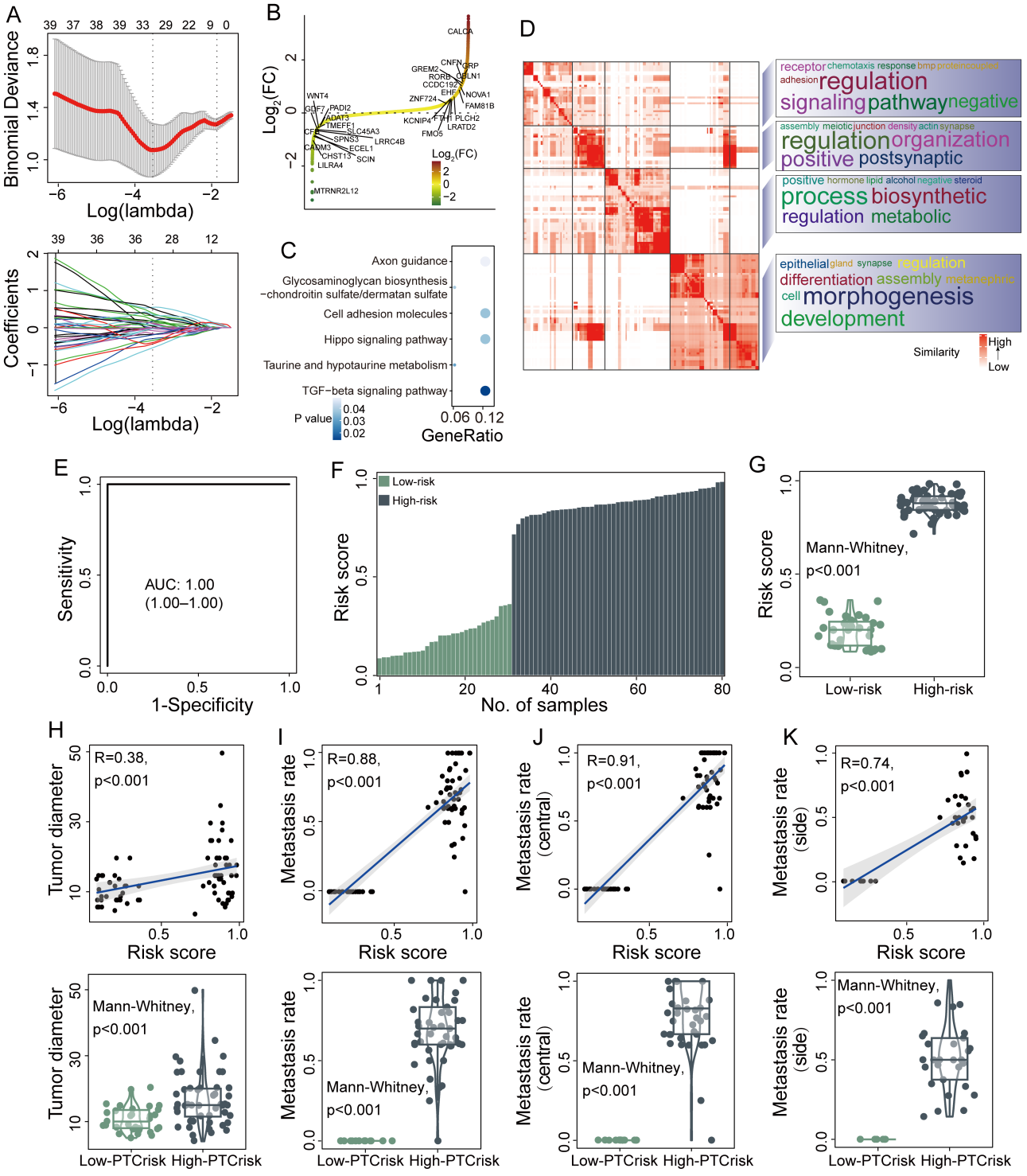

Figure 3. Legend on next page.

Further external validation of PTCrisk in multicenter cohorts

Further external validation of PTCrisk was conducted in 495 patients in TCGA, using TNM classifications to examine risk scores' association with cancer progression [29]. Notably, PTCrisk scores were significantly higher in N1 than in N0 classifications, associating higher PTCrisk scores with advanced regional lymph node spread (Fisher's test $p < 0.001$; Figure 5A). Additionally, the risk scores tended to increase from T1 to T4 classifications (Figure 5B). We also observed a progressive increase in risk scores across different stages, divided by intervals of 0.2 scores (Figure 5C). Moreover, the diagnostic performance for identifying patients with early or late clinical stages was consistent with the TNM staging results, with higher scores associated with later-stage PTC (Figure 5D). Furthermore, we calculated the enrichment scores of hallmark gene sets for each sample and found significant enrichment of biological features in the predicted high-PTCrisk group (Figure 5E).

To ensure cross-platform compatibility and universal applicability of PTCrisk, we analyzed additional samples from GSE35570 (65 samples) and GSE27155 (51 samples), which were profiled using the Affymetrix GeneChip platform. BRAF-driven tumors are known to be associated with unregulated cell proliferation in thyroid cancer and may indicate an unfavorable course [30]. In both GSE35570 and GSE27155 cohorts, patients with *BRAF* mutations exhibited significantly higher risk scores compared to *BRAF*-wild type, and an increasing proportion of *BRAF*-mutated samples was observed with increasing risk scores (Figure 5F,H). Moreover, the high-PTCrisk group was characterized by high activation of hallmark gene sets (Figure 5G). Collectively, these findings across diverse cohorts and platforms further confirmed the reliable and universal diagnostic performance of the PTCrisk model.

Identification and validation of potential prognostic biomarkers

Using univariate Cox regression analysis with the expression of DEGs as a continuous variable in the WMU-1 cohort, we identified 10 genes significantly correlated with patient survival ($p < 0.1$; Figure 6A). Subsequently, we independently validated three of these genes (*GREM2*, *EMILIN1*, *PYCR1*) in the TCGA cohort ($p < 0.1$; Figure 6B). Further Kaplan–Meier survival analysis revealed that high expression levels of *GREM2*, *EMILIN1*, and *PYCR1* were significantly associated with both progression-free survival and overall survival (log-rank $p < 0.001$; Figure 6C,D). To assess the prognostic potential of these three genes, risk classification analyses were conducted in both the WMU-1 and TCGA cohorts. The AUC values for predicting 5-year survival were 0.78, 0.75, and 0.88 in the WMU-1 cohort, and 0.62, 0.58, and 0.64 in the TCGA cohort for *GREM2*, *EMILIN1*, and *PYCR1*, respectively (Figure 6E,F). These compelling results demonstrate *GREM2*, *EMILIN1*, and *PYCR1* as promising prognostic biomarkers capable of effectively predicting the clinical outcomes of PTC patients.

Discussion

In the present study, we performed a comprehensive transcriptomic characterization of 113 PTC specimens from our institute to investigate the molecular and immunological features and their implications for diagnostic and prognostic purposes. Previous studies on the immune microenvironment of tumors have elucidated the intricacies of cancer immunoediting, a dynamic process characterized by the interaction of the immune system with evolving tumors and consisting of three phases: elimination, equilibrium, and escape [31,32]. Transcriptomic and functional

Figure 3. Discovery of candidate biomarkers for potential PTC progression and establishment of a model for PTC diagnosis. (A) Identification of the influencing variables by least absolute shrinkage and selection operator (LASSO) regression and 31 variables selected for further analysis. The plot shows the coefficients of each predictor. (B) Genes are ranked according to $\log_2$ fold change, and selected predictors are highlighted. (C) The corresponding enrichment pathways are shown for the 31 variables. The point size and color represent the number of DEGs in the pathway and the significance level. (D) Semantic similarity matrix of clustering of gene ontology biological process terms and annotation with word clouds. (E) ROC curve analysis to assess the performance of risk prediction of the model in the WMU-1 cohort. (F) The score distribution and status of the patients are sorted according to their increasing risk score. (G) Boxplot for predicting risk scores between the high- and low-risk groups. (H–K) Pearson correlation and boxplot showing between (H) tumor diameter, (I) lymph node metastasis rates, (J) central lymph node metastasis rates, (K) lateral lymph node metastasis rates, and predicting risk scores or high- and low-PTCrisk groups. The data were analyzed using the Mann–Whitney *U* test. AUC, the area under the curve; ROC, receiver-operating characteristic.

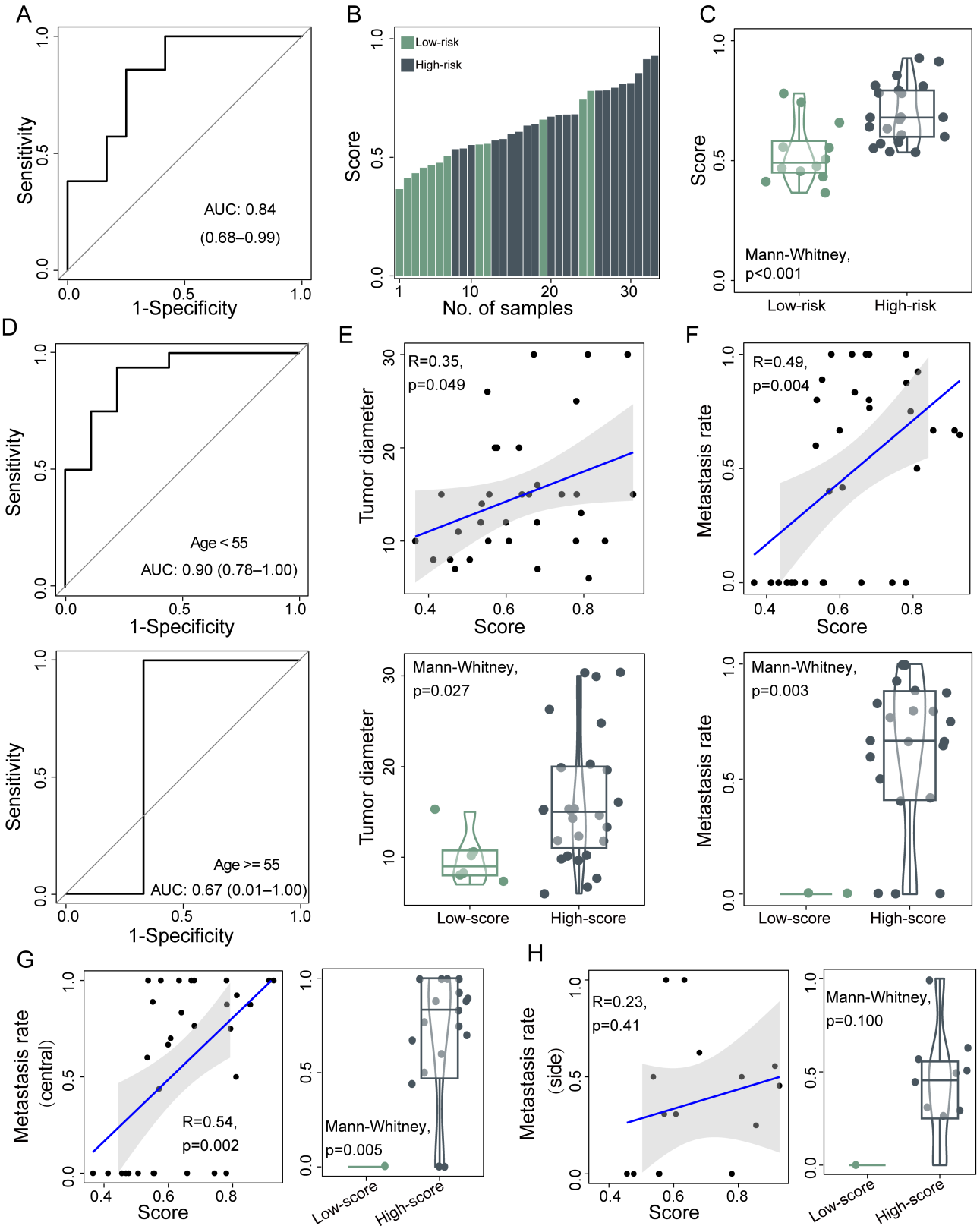

Figure 4. Legend on next page.

analysis of high-risk PTC patients revealed a significant enrichment of hallmark gene sets compared to the low-risk patients, suggesting that the immune system in high-risk patients is more likely to be engaged in the escape phase, a critical period during which tumor cells evade immune detection and control. In addition, the significant enrichment of developmental and signaling pathways suggested rapid proliferation and spread of tumor cells in high-risk PTC. Conversely, our findings in low-risk PTC patients show a higher presence of both pro- and anti-tumor immune responses, suggesting that the immune system in low-risk patients primarily functions in the equilibrium phase. The detection of anti-tumor immune responses during this equilibrium underscores the persistent efforts of the immune system to counteract tumor expansion, which plays a critical role in improving the prognosis of low-risk patients by slowing the pace of disease progression.

The genome-wide screening was conducted using LASSO regression, revealing 31 critical genes associated with morphogenesis, development, and biosynthesis, highlighting their significance in cancer pathogenesis. Specifically, overexpression of *CALCA* and *GRP* has been observed across various tumor types, including thyroid cancer, while MTRNR2L12 has been implicated in inhibiting the execution phase of apoptosis [33,34]. Although these current pieces of knowledge enhance our understanding of the identified genes, their clinically applicable values in PTC diagnosis warrant further exploration. Therefore, we developed a diagnostic model named PTCrisk, which generates a probabilistic scale ranging from 0.0 to 1.0, potentially aiding in clinical risk assessment. The effectiveness and reliability of PTCrisk were evaluated across both internal and external multicenter cohorts, demonstrating remarkable diagnostic accuracy across diverse detection platforms and patient populations. Significantly, thyroid cancer incorporates patient age into disease staging in various staging systems, such as the American Joint Committee on Cancer, highlighting the significance of patient age for risk stratification in thyroid cancer [8,35,36]. Therefore, by segregating samples into distinct age groups, we observed high diagnostic performance in both groups. We also unveiled a positive correlation between PTCrisk scores and key clinicopathological features, such as metastatic rates and tumor diameter. Similarly, external cohort analyses revealed congruent associations with TNM stages and *BRAF* mutation status, alongside an observable gradation in risk scores across different stages. These findings suggest the potential utility of PTCrisk in guiding clinical decision-making.

Furthermore, our identification of *GREM2*, *EMILIN1*, and *PYCR1* as survival-associated genes through Cox regression analysis, with subsequent validation in the TCGA cohort, introduces novel prognostic biomarkers for PTC. It has been reported that GREM2 may serve as a potential biomarker for medullary thyroid cancer prognosis, as it is one of the genes that are commonly dysregulated in both rat and human medullary thyroid cancer [37]. Although there is no evidence that *EMILIN1* and *PYCR1* are associated with thyroid cancer survival, high expression is unfavorable in renal cancer or liver cancer based on cell line data from the Human Protein Atlas [34].

Several limitations to this study should be acknowledged. First, the clinical relevance of the identified genes in the diagnosis of PTC remains to be established. Further research is needed to determine their practical utility in a clinical setting to translate research findings into clinical applications, which would involve evaluating their diagnostic accuracy, reliability, and predictive value in real-world clinical scenarios. Second, further validation of prognostic biomarkers requires verification in a larger population cohort from multiple institutions to ensure robustness and generalizability.

In conclusion, this study profiled the comprehensive transcriptomic landscape of 113 Chinese PTC patients and demonstrated that molecular and biological features contribute to risk stratification and clinical behavior variability in PTCs. Furthermore, we derived and validated a 31-gene transcriptomic-based signature (PTCrisk) that is highly predictive of risk levels. These findings provide further molecular insights into patient risk stratification and may further advance personalized treatments for PTC.

Figure 4. Performance of the diagnostic model in the validation cohort. (A) ROC plot with its 95% confidence interval presenting the performance of the model in the WMU-2 cohort. (B) The score distribution and status of the patients sorted according to their increasing risk score. (C) Boxplots showing the distribution of the risk score in high- and low-risk patients. (D) ROC curve and AUC value of the model for identifying patients' status in the age ≥55 and age <55 groups. (E–H) Pearson correlation and boxplot showing between (E) tumor diameter, (F) lymph node metastasis rates, (G) central lymph node metastasis rates, (H) lateral lymph node metastasis rates, and predicting risk scores for high- and low-PTCrisk groups. Statistical significance is determined using the Mann–Whitney *U* test. AUC, the area under the curve; ROC, receiver-operating characteristic.

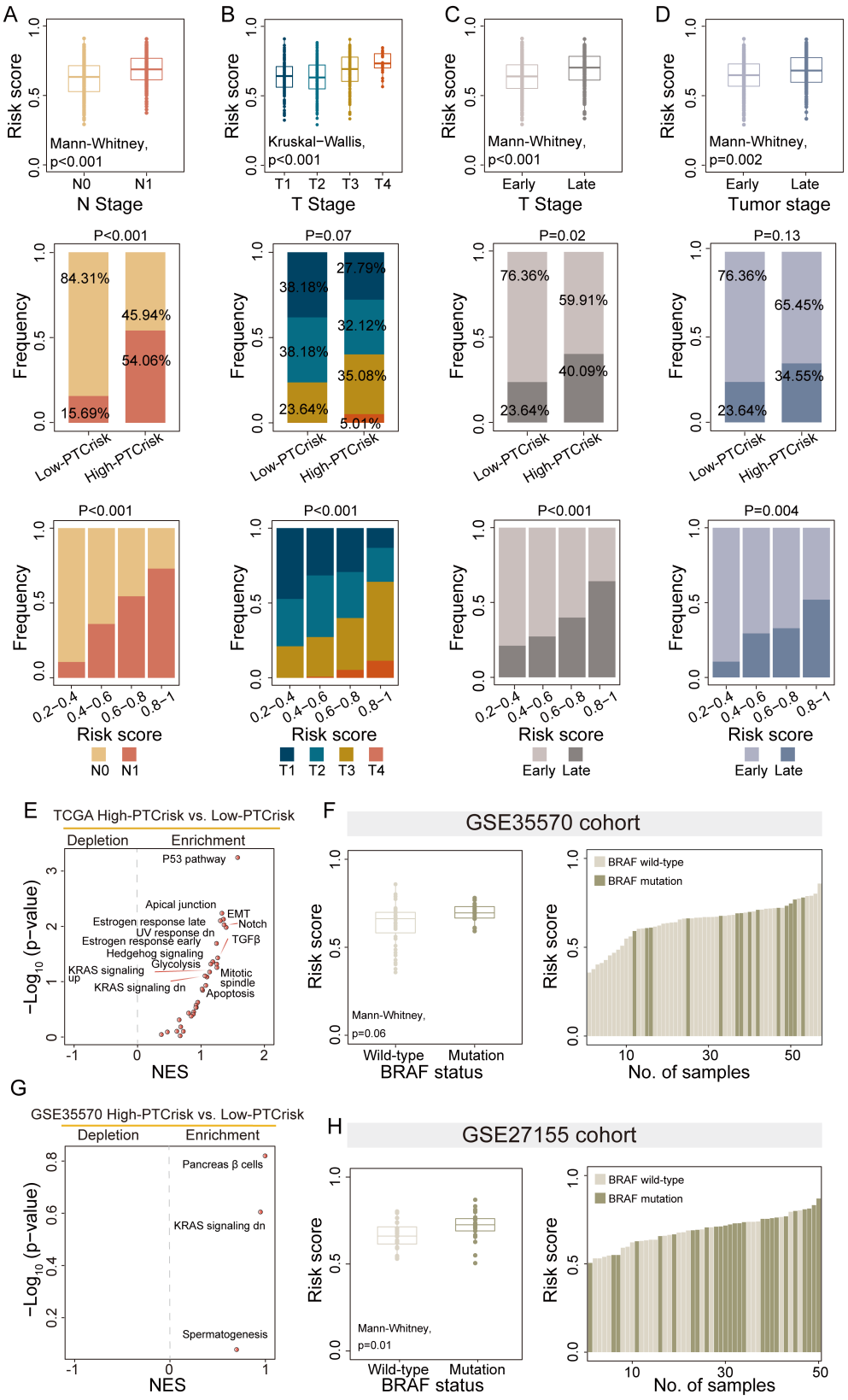

Figure 5. Legend on next page.

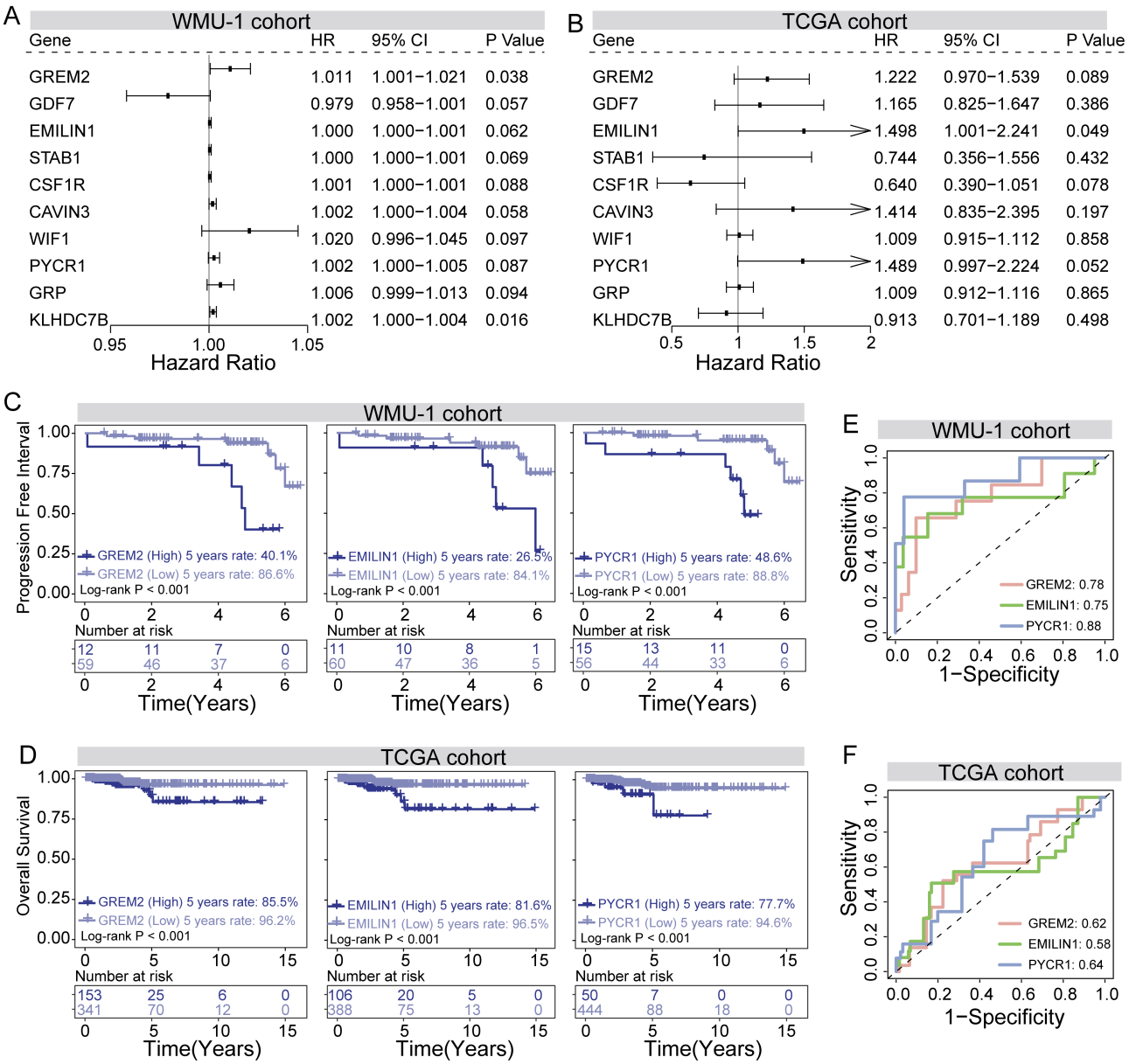

Figure 6. Performance of biomarkers in identifying individual PTC patient prognoses. (A, B) Forest plots depicting the hazard ratio and 95% confidence intervals derived from candidate genes' univariate survival analysis in (A) the WMU-1 cohort and (B) TCGA. (C, D) Kaplan–Meier survival curves of patients between the high and low expression of *GREM2*, *EMILIN1*, and *PYCR1* in (C) the WMU-1 cohort and (D) TCGA. The *p* values were calculated using the log-rank test. (E, F) The AUCs of the timeROC curves at 5 years for the three genes in (E) the WMU-1 cohort and (F) TCGA showing the prognostic performance. AUC, area under the curve; timeROC, time-dependent receiver-operating characteristic.

Figure 5. Independent validation of the model in external multicenter cohorts. (A–D) The upper panels illustrate the distribution of risk scores for patients in different clinical stages (N stage, T stage, and tumor stage). The Mann–Whitney *U* test or Kruskal–Wallis test was used to assess the statistical significance. The middle panels show the frequency distribution of stages across low- and high-PTC risk groups. The statistical significance of the proportional bar was determined using the Fisher's test. The lower panels display the frequency distribution of risk scores across different risk score intervals for different clinical stages. (E, G) Volcano plots showing the enrichment of hallmark gene sets of samples in two different groups derived from risk scores in (E) the TCGA cohort and (G) the GSE35570 cohort. (F, H) Comparison of the risk score in (F) the GSE35570 cohort and (H) between *BRAF* mutation and wildtype. The score distribution and *BRAF* mutation status of the patients are sorted according to their increasing risk score.

Acknowledgements

This study was supported by the Major Science and Technology Innovation Program of Wenzhou (Grant No. ZY2022008, ZY2021008).

Author contributions statement

MZ and OW conceptualized and supervised the study. CY analyzed the data. CZ, JL, XW, XM, CL and SS contributed to sample collection and carried out experiments. CY, CZ and MZ wrote the manuscript. All authors approved the final manuscript.

Data availability statement

The whole transcriptome sequencing data of 113 cases have been deposited in the National Genomics Data Center (NGDC) (https://ngdc.cncb.ac.cn/; project ID: OMIX006055). The external validation cohorts were publicly available in TCGA (https://xenabrowser.net/) and GEO (https://www.ncbi.nlm.nih.gov/geo).

References

1. Wiltshire JJ, Drake TM, Uttley L, *et al*. Systematic review of trends in the incidence rates of thyroid cancer. *Thyroid* 2016; **26:** 1541–1552.
2. Sung H, Ferlay J, Siegel RL, *et al*. Global cancer statistics 2020: GLOBOCAN estimates of incidence and mortality worldwide for 36 cancers in 185 countries. *CA Cancer J Clin* 2021; **71:** 209–249.
3. Laha D, Nilubol N, Boufraqech M. New therapies for advanced thyroid cancer. *Front Endocrinol* 2020; **11:** 82.
4. Lundgren CI, Hall P, Dickman PW, *et al*. Clinically significant prognostic factors for differentiated thyroid carcinoma: a population-based, nested case-control study. *Cancer* 2006; **106:** 524–531.
5. La Vecchia C, Malvezzi M, Bosetti C, *et al*. Thyroid cancer mortality and incidence: a global overview. *Int J Cancer* 2015; **136:** 2187–2195.
6. Qu H, Sun G, Liu Y, *et al*. Clinical risk factors for central lymph node metastasis in papillary thyroid carcinoma: a systematic review and meta-analysis. 2015; **83:** 124–132.
7. Lloyd RV, Buehler D, Khanafshar E. Papillary thyroid carcinoma variants. *Head Neck Pathol* 2011; **5:** 51–56.
8. Shi X, Liu R, Basolo F, *et al*. Differential clinicopathological risk and prognosis of major papillary thyroid cancer variants. *J Clin Endocrinol Metab* 2016; **101:** 264–274.
9. Lim H, Devesa SS, Sosa JA, *et al*. Trends in thyroid cancer incidence and mortality in the United States, 1974–2013. *JAMA* 2017; **317:** 1338–1348.
10. Pacini F, Fuhrer D, Elisei R, *et al*. ETA consensus statement: what are the indications for post-surgical radioiodine therapy in differentiated thyroid cancer? *Eur Thyroid J* 2022; **11:** e210046.
11. Abelleira E, Jerkovich F. Dynamic risk assessment in patients with differentiated thyroid cancer. *Rev Endocr Metab Disord* 2024; **25:** 79–93.
12. Haugen BR, Alexander EK, Bible KC, *et al*. 2015 American Thyroid Association management guidelines for adult patients with thyroid nodules and differentiated thyroid cancer: the American Thyroid Association guidelines task force on thyroid nodules and differentiated thyroid cancer. *Thyroid* 2016; **26:** 1–133.
13. Handkiewicz-Junak D, Swierniak M, Rusinek D, *et al*. Gene signature of the post-Chernobyl papillary thyroid cancer. *Eur J Nucl Med Mol Imaging* 2016; **43:** 1267–1277.
14. Giordano TJ, Kuick R, Thomas DG, *et al*. Molecular classification of papillary thyroid carcinoma: distinct BRAF, RAS, and RET/PTC mutation-specific gene expression profiles discovered by DNA microarray analysis. *Oncogene* 2005; **24:** 6646–6656.
15. Gautier L, Cope L, Bolstad BM, *et al*. affy – analysis of Affymetrix GeneChip data at the probe level. *Bioinformatics* 2004; **20:** 307–315.
16. Kuhn M. Building predictive models in R using the caret package. *J Stat Softw* 2008; **28:** 1–26.
17. Love MI, Huber W, Anders S. Moderated estimation of fold change and dispersion for RNA-seq data with DESeq2. *Genome Biol* 2014; **15:** 550.
18. Bindea G, Mlecnik B, Hackl H, *et al*. ClueGO: a Cytoscape plug-in to decipher functionally grouped gene ontology and pathway annotation networks. *Bioinformatics* 2009; **25:** 1091–1093.
19. Shannon P, Markiel A, Ozier O, *et al*. Cytoscape: a software environment for integrated models of biomolecular interaction networks. *Genome Res* 2003; **13:** 2498–2504.
20. Gu Z, Hubschmann D. simplifyEnrichment: a Bioconductor package for clustering and visualizing functional enrichment results. *Genomics Proteomics Bioinformatics* 2023; **21:** 190–202.
21. Wu T, Hu E, Xu S, *et al*. clusterProfiler 4.0: a universal enrichment tool for interpreting omics data. *Innovation (Camb)* 2021; **2:** 100141.
22. Newell F, Pires da Silva I, Johansson PA, *et al*. Multiomic profiling of checkpoint inhibitor-treated melanoma: identifying predictors of response and resistance, and markers of biological discordance. *Cancer Cell* 2022; **40:** 88–102.e107.
23. Liberzon A, Birger C, Thorvaldsdottir H, *et al*. The Molecular Signatures Database (MSigDB) hallmark gene set collection. *Cell Syst* 2015; **1:** 417–425.
24. Hanzelmann S, Castelo R, Guinney J. GSVA: gene set variation analysis for microarray and RNA-seq data. *BMC Bioinformatics* 2013; **14:** 7.
25. Yang L, Zhang Z, Dong J, *et al*. Multi-dimensional characterization of immunological profiles in small cell lung cancer uncovers clinically relevant immune subtypes with distinct prognoses and therapeutic vulnerabilities. *Pharmacol Res* 2023; **194:** 106844.
26. Zhang Z, Sun X, Liu Y, *et al*. Spatial transcriptome-wide profiling of small cell lung cancer reveals intra-tumoral molecular and subtype heterogeneity. *Adv Sci (Weinh)* 2024; **11:** e2402716.
27. Shaha AR, Shah JP, Loree TR. Risk group stratification and prognostic factors in papillary carcinoma of thyroid. *Ann Surg Oncol* 1996; **3:** 534–538.

28. Edge SB, Compton CC. The American Joint Committee on Cancer: the 7th edition of the AJCC cancer staging manual and the future of TNM. *Ann Surg Oncol* 2010; **17:** 1471–1474.
29. Rosen RD, Sapra A. *TNM Classification*. StatPearls: Treasure Island, FL, 2024.
30. Caronia LM, Phay JE, Shah MH. Role of BRAF in thyroid oncogenesis. *Clin Cancer Res* 2011; **17:** 7511–7517.
31. Vesely MD, Schreiber RD. Cancer immunoediting: antigens, mechanisms, and implications to cancer immunotherapy. *Ann N Y Acad Sci* 2013; **1284:** 1–5.
32. Dunn GP, Bruce AT, Ikeda H, *et al*. Cancer immunoediting: from immunosurveillance to tumor escape. *Nat Immunol* 2002; **3:** 991–998.
33. Hashimoto Y, Niikura T, Tajima H, *et al*. A rescue factor abolishing neuronal cell death by a wide spectrum of familial Alzheimer's disease genes and Abeta. *Proc Natl Acad Sci U S A* 2001; **98:** 6336–6341.
34. Uhlen M, Fagerberg L, Hallstrom BM, *et al*. Proteomics. Tissue-based map of the human proteome. *Science* 2015; **347:** 1260419.
35. American Thyroid Association Guidelines Taskforce on Nodules and Differentiated Thyroid Cancer, Cooper DS, *et al*. Revised American Thyroid Association management guidelines for patients with thyroid nodules and differentiated thyroid cancer. *Thyroid* 2009; **19:** 1167–1214.
36. Lang BH, Lo CY, Chan WF, *et al*. Prognostic factors in papillary and follicular thyroid carcinoma: their implications for cancer staging. *Ann Surg Oncol* 2007; **14:** 730–738.
37. Molatore S, Kugler A, Irmler M, *et al*. Characterization of neuroendocrine tumors in heterozygous mutant MENX rats: a novel model of invasive medullary thyroid carcinoma. *Endocr Relat Cancer* 2018; **25:** 145–162.

SUPPLEMENTARY MATERIAL ONLINE

Figure S1. Correlation heatmap of immunological features

Table S1. List of differentially expressed genes between high-risk and low-risk PTCs